ADVANCED MATERIALS
www.advmat.de

Imaging Field-Driven Melting of a Molecular Solid at the Atomic Scale

Franklin Liou, Hsin-Zon Tsai, Zachary A. H. Goodwin, Andrew S. Aikawa, Ethan Ha, Michael Hu, Yiming Yang, Kenji Watanabe, Takashi Taniguchi, Alex Zettl, Johannes Lischner,* and Michael F. Crommie**

Solid–liquid phase transitions are basic physical processes, but atomically resolved microscopy has yet to capture their full dynamics. A new technique is developed for controlling the melting and freezing of self-assembled molecular structures on a graphene field-effect transistor (FET) that allows phase-transition behavior to be imaged using atomically resolved scanning tunneling microscopy. This is achieved by applying electric fields to 2,3,5,6-tetrafluoro-7,7,8,8-tetracyanoquinodimethane-decorated FETs to induce reversible transitions between molecular solid and liquid phases at the FET surface. Nonequilibrium melting dynamics are visualized by rapidly heating the graphene substrate with an electrical current and imaging the resulting evolution toward new 2D equilibrium states. An analytical model is developed that explains observed mixed-state phases based on spectroscopic measurement of solid and liquid molecular energy levels. The observed nonequilibrium melting dynamics are consistent with Monte Carlo simulations.

1. Introduction

Phase transitions reflect the collective behavior of large numbers of particles but originate from rapid reconfigurations at the single-particle scale. Great progress has been made at controlling structural, electronic, and magnetic phase transitions in different materials by varying macroscopic parameters such as strain,[1–3] density,[4,5] and electromagnetic fields,[6–9] but imaging the atomic-scale dynamics of such transitions has proved difficult. The reason for this is the difficulty of combining atomic-scale microscopy with the high bandwidth required to capture fast dynamics. Here we describe a different approach for exploring dynamical processes that involve rapidly quenching the thermally-induced kinetics of 2D phase transitions and imaging their evolution toward equilibrium frame-by-frame using atomically resolved scanning tunneling microscopy (STM).

We have used this technique to image the electrostatically driven solid–liquid phase transition of 2,3,5,6-tetrafluoro-7,7,8,8-tetracyanoquinodimethane (F_4TCNQ) molecules at the surface of a graphene field-effect transistor (FET) held at cryogenic

F. Liou, H.-Z. Tsai, A. S. Aikawa, E. Ha, M. Hu, Y. Yang, A. Zettl, M. F. Crommie
Department of Physics
University of California at Berkeley
Berkeley, CA 94720, USA
E-mail: azettl@berkeley.edu; crommie@berkeley.edu

F. Liou, H.-Z. Tsai, A. S. Aikawa, A. Zettl, M. F. Crommie
Materials Sciences Division
Lawrence Berkeley National Laboratory
Berkeley, CA 94720, USA

F. Liou, A. Zettl, M. F. Crommie
Kavli Energy NanoSciences Institute at the University of California at Berkeley
Berkeley, CA 94720, USA

Z. A. H. Goodwin, J. Lischner
Department of Materials
Imperial College London
Prince Consort Rd, London SW7 2BB, UK
E-mail: j.lischner@imperial.ac.uk

Z. A. H. Goodwin
National Graphene Institute
University of Manchester
Booth St. E. Manchester M13 9PL, Manchester UK

Z. A. H. Goodwin
School of Physics and Astronomy
University of Manchester
Oxford Road, Manchester M13 9PL, UK

K. Watanabe
Research Center for Electronic and Optical Materials
National Institute for Materials Science
1-1 Namiki, Tsukuba 305-0044, Japan

T. Taniguchi
Research Center for Materials Nanoarchitectonics
National Institute for Materials Science
1-1 Namiki, Tsukuba 305-0044, Japan

The ORCID identification number(s) for the author(s) of this article can be found under https://doi.org/10.1002/adma.202300542

DOI: 10.1002/adma.202300542

temperature in ultrahigh vacuum. Voltages applied to the back gate of such a device induce reversible freezing and melting of molecular structures at the surface, but the evolution of these structures toward new equilibrium states is quenched by the device's low temperature ($T \approx 4$ K). Equilibration can only be achieved by passing current through the graphene substrate, thereby transiently raising the temperature and speeding the molecular kinetics (i.e., the diffusive motion). Rapid cooling after the current is stopped allows "snapshots" of the surface molecular configuration to be taken without the need for ultrafast imaging techniques. Stop-motion movies of field-induced molecular phase transitions can be made this way that have atomic spatial resolution and a time resolution set by the electronic and thermal relaxation time constants of the device.[10] This has allowed us to resolve the melting and freezing processes of F_4TCNQ molecules at the single-molecule level in both liquid and solid phases, something not possible via other microscopy techniques[11–13] due to the non-crystallinity and fast dynamics of molecular liquids.[11,12]

Scanning tunneling spectroscopy (STS) measurements reveal that a solid phase of F_4TCNQ is favored when the graphene Fermi level (E_F) is lowered to a point where the molecules become charge-neutral. Raising E_F sufficiently with a back-gate causes the solid F_4TCNQ phase to melt into a liquid phase in a process where each molecule converted to the liquid phase accepts a single electron. The F_4TCNQ liquid phase is thus populated by negative ions.[14] We have developed a simple theoretical framework that explains the equilibrium energetics of this first-order solid–liquid phase transition as a function of gate voltage, and have performed Monte Carlo simulations that capture its nonequilibrium melting dynamics.

2. Results

Figure 1 shows the reversible melting/freezing of a partial monolayer of F_4TCNQ on a graphene FET as it transitions through different equilibrium states in response to the applied back-gate voltage V_G. For $V_G = -30$ V (Figure 1a) the molecules all lie in a solid "chain" phase after flowing source–drain current $I_{SD} = 1$ mA through the device for 180 s (all STM images and spectroscopy are acquired only after setting I_{SD} to zero to quench molecular motion by reestablishing the device base temperature of $T = 4.5$ K). Figure 1j shows close-up STM and AFM images of the F_4TCNQ solid phase revealing two quasi-1D chain morphologies that we call "linear" and "zigzag" (more detailed structural characterization can be found in Figures S7 and S8, Supporting Information). The structure factor of the chain phase shows clear periodicity, thus indicating that it is a quasi-1D crystalline solid (see additional details in Section 8, Figure S7, Supporting Information).

Subsequent raising of the gate voltage to $V_G = 0$ V followed by application of "diffusive" conditions (i.e., by setting $I_{SD} = 1$ mA) for 180 s causes the molecular solid to partially melt. This can be seen in Figure 1b which shows isolated F_4TCNQ molecules dotting the surface near the edge of the solid phase in the same area as Figure 1a (the isolated molecules belong to a 2D liquid phase as described below). This is an equilibrium configuration in the sense that the average concentrations of the liquid and solid phases have stopped changing with time under diffusive conditions. The images in Figure 1c,d show the equilibrium configurations of the same region after incrementally raising the gate voltage first to $V_G = 6$ V and then to $V_G = 30$ V under diffusive conditions. For every step increase in V_G, the solid is seen to melt a little more until it is completely liquefied at $V_G = 30$ V. Figure 1e–h shows the same surface region as V_G is decreased back to -30 V under identical diffusive conditions. The liquid–solid phase transition is completely reversible (movies of the freezing/melting processes are shown in Movies S1 and S2, Supporting Information).

Justification for calling the phase containing isolated molecules (Figure 1d) a liquid comes from an analysis of the molecular radial distribution function, $g(r)$, and structure factor, $S(q)$. Figure 1k shows $g(r)$ extracted from a large-area image containing isolated molecules prepared under equilibrium conditions (see Section 1, Supporting Information for additional details). $g(r)$ shows evenly spaced peaks with a spacing of $a = 3.84$ nm, as expected for the shell structure of an isotropic liquid.[15] The structure factor seen in the Figure 1k inset (for the same STM image) is also indicative of an isotropic liquid and shows no evidence of crystal or gas behavior.[15]

Understanding the cause of the observed molecular phase transition requires understanding how charge transfers between molecules and graphene under different gating conditions. STS measurements were used to gain insight into this process by separately measuring the local electronic structure of the solid and liquid phases. **Figure 2**a shows dI/dV spectra measured on an F_4TCNQ chain (solid phase) compared to an isolated F_4TCNQ molecule (liquid phase) for $V_G = -60$ V (this is the hole-doped graphene regime as shown by the inset electronic structure diagram in Figure 2a). The bare graphene spectrum for this surface (taken 10 nm away from any molecules) is shown in the inset for reference. A dip in the bare graphene local density of states near $V = 0.34$ V marks the location of the graphene Dirac point (E_D), thus verifying that the graphene is in the hole-doped regime for this gate voltage. The gap-like feature at $V = 0$ (E_F) arises from a well-known phonon-assisted inelastic tunneling effect.[16]

The blue curve in Figure 2a shows the dI/dV spectrum for a single, isolated F_4TCNQ molecule (SM) in this hole-doped regime. The leading edge of the first peak marks the lowest unoccupied molecular orbital (LUMO) energy as discussed in previous work[14,17] ($E_L^{SM} = 0.2$ eV and is marked by a dashed blue line), while the second peak ($V_b \approx 0.4$ V) is a phonon satellite arising from intramolecular vibrations.[17] The F_4TCNQ LUMO level is unoccupied for this value of V_G. The second curve (red) shows the dI/dV spectrum measured with the STM tip held over the end molecule of an F_4TCNQ solid chain (the chain end (CE) as shown in Figure 1j). The CE spectrum is nearly identical to the single molecule spectrum except that E_L is shifted up by 0.06 eV. The third curve (orange) shows the spectrum for a molecule in the middle of a chain (CM) (as shown in Figure 1j). Here E_L is pushed up even further by an additional 0.05 eV. The overall energy-level structure is schematically represented by the inset sketch which shows the energy level alignment of the SM LUMO, the CE LUMO, and the CM LUMO relative to E_D and E_F (the experimental energy levels of the zigzag and linear chains are identical, as shown in Figure S9, Supporting Information).

This energy-level structure has important consequences for F_4TCNQ/graphene solid–liquid phase transitions. For example, suppose that V_G was first set to $V_G = -60$ V (the case shown

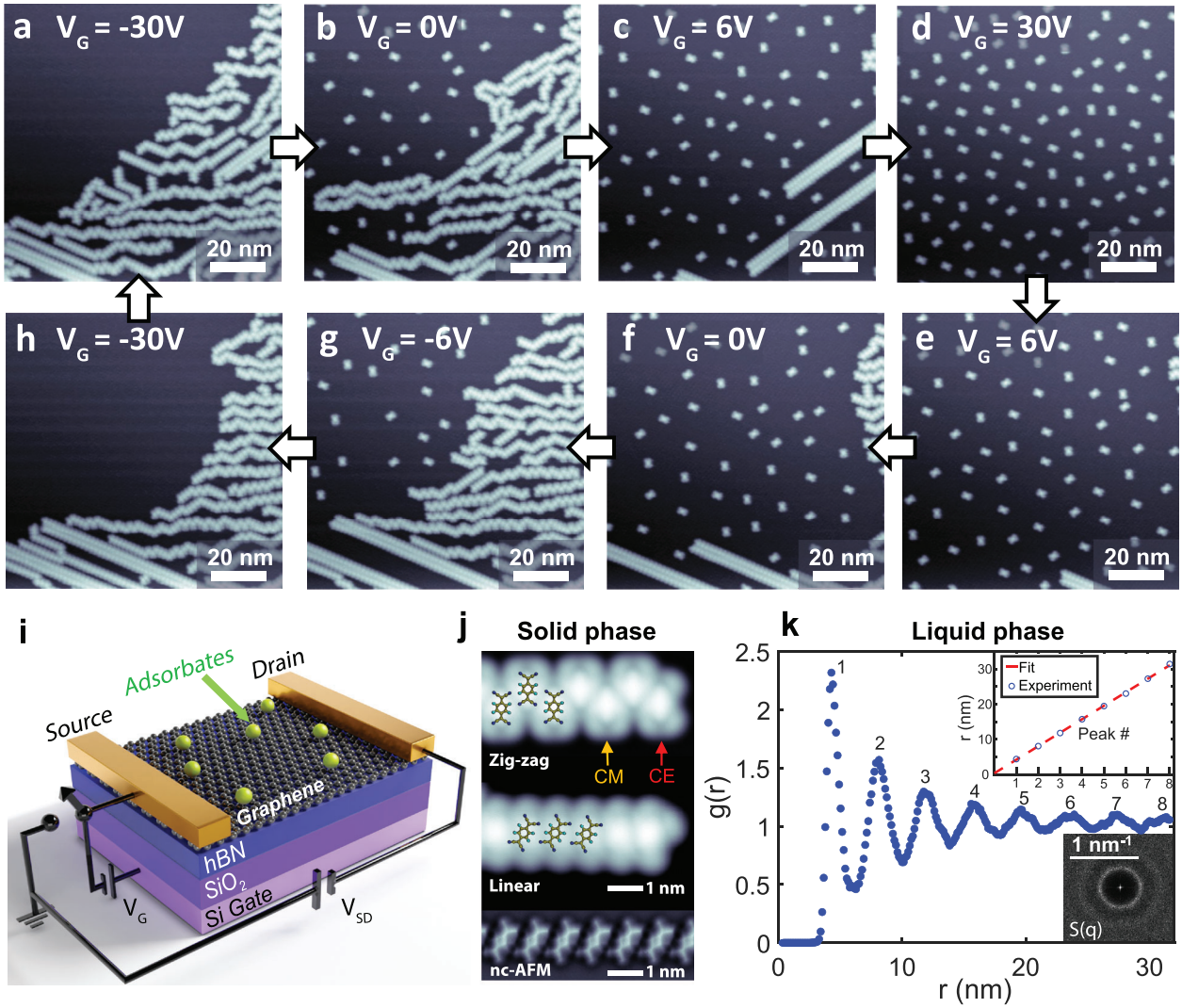

Figure 1. Gate-tunable solid–liquid molecular phase transition. a–d) STM images show the melting of self-assembled chains of F_4TCNQ molecules (solid phase) into isolated molecules (liquid phase) as V_G is increased through −30 V (a), 0 V (b), 6 V (c), 30 V (d). e–h) The reverse phase transition (liquid to solid) is observed at the same spot on the surface with molecules coalescing from the liquid phase into self-assembled chains as V_G is decreased through 6 V (e), 0 V (f), −6 V (g), −30 V (h). i) Schematic of the experimental setup shows F_4TCNQ molecules adsorbed onto the surface of a graphene FET device. j) Closeup STM images of the solid molecular chain phase (with structural overlays) show two observed geometries (linear and zig-zag), both having a center-to-center molecular distance of 8.5 Å. A bond-resolved nc-AFM image in the bottom row (obtained with a CO tip[21]) reveals the linear geometry in greater detail. k) The radial distribution function $g(r)$ of molecular positions in the liquid phase shows shell-like structure having an average shell spacing of 3.84 nm (the corresponding STM image can be seen in Figure S1b, Supporting Information). The corresponding structure factor $S(q)$ shown in the inset indicates that the liquid is isotropic. STM images were obtained at $T = 4.5$ K.

in Figure 2a) and then slowly increased under diffusive conditions. This would cause E_F to slide to the right and eventually intersect E_L^{SM}. The first molecules to fill with charge due to the increasing V_G would thus be isolated F_4TCNQ molecules. As shown previously,[14] under these conditions E_F becomes pinned close to E_L^{SM} and so never reaches the chain orbitals (E_L^{CE} or E_L^{CM}) which therefore remain charge-neutral (i.e., unoccupied) for a wide range of V_G values. Increasing V_G while E_F is pinned in this way causes molecules to melt from the neutral solid and to fill with charge, thereby increasing the molecular density of the charged liquid phase (separation between the isolated molecules is explained by Coulomb repulsion).

A useful thermodynamic variable to characterize this process is the total charge density in the molecule-decorated graphene system, $-\Delta Q$ (this counts the excess density of electrons). When the molecular chains begin to melt in response to increased V_G, $-\Delta Q$ exhibits a discontinuous jump when plotted as a function of E_F as shown in Figure 2b. Here $-\Delta Q$ is obtained from the relationship $-\Delta Q = CV_G$ where C is the capacitance per area between the graphene and the gate electrode. E_F and E_D are measured as a function of V_G from STM spectroscopy (by fitting dI/dV spectra such as that shown in the inset to Figure 2a), and the discontinuity in $-\Delta Q$ is observed to occur at $E_F - E_D \approx -0.125$ eV. For $E_F - E_D < -0.125$ eV the molecules

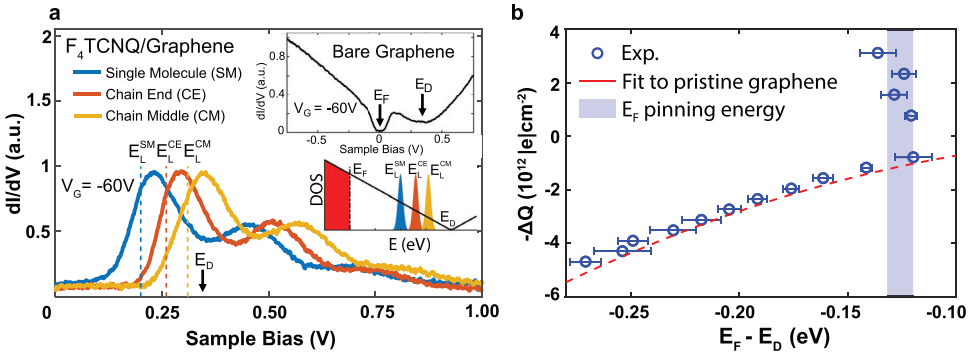

Figure 2. Electronic energy level alignment and charge accumulation under electrostatic gating. a) d*I*/d*V* spectra taken at $V_G = -60$ V for F_4TCNQ molecules at a chain middle (CM), a chain end (CE), and for single, isolated molecules (SM) (images shown in Figure 1). The inset plot shows the d*I*/d*V* spectrum measured on bare graphene for $V_G = -60$ V. The inset sketch shows the relative energy alignments of the CM LUMO state, the CE LUMO state, the SM LUMO state, the Fermi energy (E_F), and the Dirac point (E_D). b) Total charge density accumulated in the molecule/graphene surface (measured capacitively and plotted in terms of electron density) as a function of $E_F - E_D$ (as determined by STS). A discontinuity is seen at $E_F - E_D = -0.125$ eV. STS spectra obtained at $T = 4.5$ K.

are in the charge-neutral chain phase where increases in $-\Delta Q$ reflect the filling of the graphene Dirac band (thus leading to a well-known parabolic dependence of $-\Delta Q$ on E_F in graphene).[18] When E_F reaches the critical value of $E_F - E_D = -0.125$ eV, however, charge begins to flow into the F_4TCNQ LUMO states as the chain phase melts to accommodate added charge. The molecules have a high quantum capacitance at this energy and so device charge accumulates rapidly with increasing $E_{F,}$ thus resulting in discontinuous behavior as shown in Figure 2b. While the discontinuity in $-\Delta Q$ reflects the electronic part of the phase transition, concurrent imaging of molecular chain dissociation (i.e., molecular melting) shows that this electronic change accompanies the structural phase transition. The E_F dependence of $-\Delta Q$ in Figure 2b is reminiscent of the temperature dependence of transferred heat in a standard temperature-driven solid–liquid melting transition (such as ice to water), where latent heat must be provided to increase entropy as the solid converts to a liquid. Here E_F is analogous to temperature and the number of excess electrons ($-\Delta Q$) is analogous to entropy, so one can think of "latent charge" as being necessary to induce 2D molecular melting in our devices (see Section 10, Supporting Information for more detailed discussions of this analogy). Similar thermodynamic models of electrostatically driven phase transitions have been utilized to explain solid–solid phase transitions in 2D materials.[19]

These insights enable us to develop a theoretical model for quantitatively understanding the microscopic energetics of the F_4TCNQ/graphene solid–liquid phase transition. We first note that the F_4TCNQ molecules and graphene both exchange electrons with the gate which acts as a reservoir. The thermodynamics of such an open system for electrons is described by the grand potential (see Section 10, Supporting Information for a more detailed discussion). Under our low-temperature experimental conditions (which rise to ≈25 K when $I_{SD} \neq 0$) the entropy contribution TS to the grand potential is expected to be small, and so we model the grand potential as follows:

$$\Phi = U - E_F N_e \quad (1)$$

Here U is the total energy of the graphene plus molecules and N_e is the total number of electrons in the graphene/molecule system relative to a reference state. The reference here is the configuration where all electrons occupy graphene band states with energy $E < E_L^{SM}$ and the molecules are uncharged. Since the LUMO energy of the chains is higher than that of isolated molecules, we ignore the possibility of the chains becoming charged and assume that electrons occupy either single-molecule LUMO states or graphene Dirac band states. The graphene contribution to the total energy relative to the reference state is denoted by $U_g(E_F) = \int_{E_L}^{E_F} \varepsilon g(\varepsilon)\, d\varepsilon$, where $g(\varepsilon)$ is found from the well-known linear band model[20] to be $g(\varepsilon) = 2A(E_D - \varepsilon)/\pi\hbar^2 v_F^2$ (here E_D is the Dirac point energy, A is the area of graphene, and v_F is the Fermi velocity). If we assume that our system has a total of N molecules that are all in the neutral chain phase, then the molecular energy can be approximated as $U_s(N) \approx -\alpha N$ where $-\alpha$ corresponds to the energy per bond between adjacent molecules. We denote the number of electrons in this pure solid phase as $N_{e,s}$, in which case the grand potential is

$$\Phi_s = U_s\ (N) + U_g\left(E_F\right) - E_F N_{e,s} \quad (2)$$

On the other hand, if the N molecules are all in the charged liquid phase then the molecules are each charged by one electron in the LUMO and the molecular contribution to the total energy becomes $U_l(N) = E_L N$ (for simplicity we have dropped the superscript "SM" from E_L). We denote the number of electrons in this pure liquid phase as $N_{e,l}$, in which case the grand potential is

$$\Phi_l = U_l\ (N) + U_g\left(E_F\right) - E_F N_{e,l} \quad (3)$$

The critical Fermi level (E_F^c) at which the phase transition occurs is determined by setting $\Phi_s = \Phi_l$. At this Fermi level $N_{e,l} - N_{e,s} = N$ since N electrons are needed to charge the molecules, thereby yielding $E_F^c = E_L + \alpha$. For $E_F < E_F^c$ all of the electrons reside in graphene band states and all of the molecules are condensed into solid chains due to the energy gain of bond formation. For $E_F > E_F^c$, on the other hand, all of the molecules are in the charged liquid state. The transition from the solid phase to the liquid phase

does *not* occur when $E_F = E_L$ because melting the chains requires extra energy to break the bond between a chain end molecule and its neighbor (i.e., the latent heat of melting). The process of adding a charged, isolated molecule to the liquid phase only becomes energetically favorable when the Fermi level reaches a value equal to E_L plus the energy required to break one bond (α). This insight allows us to, in principle, experimentally obtain α by comparing the measured value of E_F^c at which the phase transition occurs (which is marked by Fermi level pinning) to spectroscopic measurements of E_L. Experimentally we observe E_F^c to be 120 ± 20 meV below the Dirac point energy and E_L to be 140 ± 5 meV below the Dirac point (E_L was determined previously[14]). The difference between these quantities is on the order of our experimental uncertainty, and so we are not yet able to extract an accurate value of α from our data. We are, however, able to place an upper limit on α: $\alpha \leq 40$ meV (which is consistent with a DFT-based estimate of α, see Section 5b, Supporting Information).

While the grand potential is continuous at the phase transition, its first derivative with respect to E_F is not. From Equations (2) and (3) we see that $\frac{\partial \Phi_l}{\partial E_F}$ and $\frac{\partial \Phi_s}{\partial E_F}$ differ by N at $E_F = E_F^c$, confirming that this is a first-order phase transition. In a heat-driven first-order phase transition, such as the transformation of ice to liquid water, latent heat is required to convert the phases at the transition temperature. Our phase transition, however, is not heat-driven but is rather driven by electrostatic gating. There is thus a latent charge of N electrons required for complete conversion of N molecules in the solid phase to the liquid phase rather than a latent heat. This is consistent with the experimental discontinuity in $-\Delta Q$ seen in Figure 2b which reflects the charge transferred to melt F_4TCNQ while E_F is pinned at the critical value, analogous to how latent heat is transferred to melt a solid while the temperature is pinned at the melting point in a heat-driven solid–liquid phase transition.

The preceding discussion is relevant for equilibrium conditions of the pure liquid phase ($E_F > E_F^c$) vs the pure solid phase ($E_F < E_F^c$), but we are also able to characterize the nonequilibrium solid–liquid (mixed phase) coexistence regime (i.e., unstable excursions from $E_F = E_F^c$) where the proportion of molecules in the chain and liquid phases can be adjusted from one equilibrium state to another (**Figure 3**). Figure 3a shows a plot of the experimental liquid phase molecular density (N_l/A, where A is the graphene area) vs $V_G - V_0$ where $V_0 = -10$ V is the gate voltage at which isolated molecules first appear in STM images. The yellow dots in Figure 3a shows that the experimental equilibrium values for N_l/A exhibit a linear dependence on gate voltage. The magenta dots, on the other hand, show experimental nonequilibrium data obtained by changing V_G and I_{SD} in such a way that diffusive conditions do not last long enough for the system to fully equilibrate. Figure 3b–g shows a full cycle of the system (measured at a single location on the device) as it evolves from one equilibrium configuration to a different one (yellow dots) and then back again by transitioning through a series of intermediate nonequilibrium states (magenta dots).

To understand this experimental process, we start with Figure 3b which shows a patch of the surface that was initially in an equilibrium state at $V_G - V_0 = 60$ V. At this gate voltage a relatively high liquid phase density ($N_l/A = 4.1 \times 10^{12}$ molecules per cm^2) coexists with a much lower concentration of the solid phase. The gate voltage was then changed to $V_G - V_0 = 50$ V under non-diffusive conditions (i.e., $I_{SD} = 0$) to set a new equilibrium target, but without allowing the system to evolve toward the new target (since the kinetics are quenched by keeping $I_{SD} = 0$). The resulting nonequilibrium configuration is denoted $t = 0$ (Figure 3b) and is visually identical to the equilibrium state at $V_G - V_0 = 60$ V. Figure 3c shows the same region after subjecting it to diffusive conditions (by setting $I_{SD} = 1.1$ mA) for $\Delta t = 50$ ms while holding the gate voltage constant at $V_G - V_0 = 50$ V. The solid phase density is seen to increase, but equilibrium is not yet established. Figure 3d shows the same region after allowing it to evolve for an additional 50 ms under diffusive conditions while maintaining $V_G - V_0 = 50$ V. The system is now in equilibrium with N_l/A reduced to 3.5×10^{12} molecules per cm^2 and the solid density correspondingly increased. Figure 3e–g show the same process in reverse as V_G is reset to the original value of $V_G - V_0 = 60$ V. The system is observed to evolve back to its original equilibrium configuration after passing through a nonequilibrium state (Figure 3f) regime.

The mixed-phase solid/liquid configurations observed in Figure 3 can be understood within our theoretical framework in a straightforward way. To do this we consider the total energy of a mixed phase state containing N_l molecules in the liquid phase and $N - N_l$ molecules in the chain phase given by

$$U\left(N_l, E_F\right) = U_l\left(N_l\right) + U_s\left(N - N_l\right) + U_g\left(E_F\right) \tag{4}$$

where U_l, U_s, U_g, and N are defined the same as for Equations (2) and (3). Here N is constant, and E_F is determined by V_G and N_l. Only N_l remains variable, and its value at equilibrium N_l^{eq} is obtained by minimizing Equation (4) with respect to N_l (see Section 4, Supporting Information for details). The resulting expression for N_l^{eq} per unit area is

$$\frac{N_l^{eq}}{A} = CV_G + \frac{|E_D - \left(E_L + \alpha\right)|^2}{\pi \hbar^2 v_F^2} \tag{5}$$

where A is the area of the graphene capacitor, E_L is the LUMO energy, E_D is the Dirac point energy, and v_F is the Fermi velocity near the Dirac point (1.1×10^6 m s^{-1}). This expression is similar to an expression derived in ref. [14] using a different approach, but the new expression differs in the last term of Equation (5) which arises due to the energy required to break a bond (α), a factor not considered in ref. [14]. Equation (5) is plotted in Figure 3a (white dashed line) and is seen to match the equilibrium data (yellow dots) quite well. The nonequilibrium behavior (magenta dots) can be explained by plotting U from Equation (4) as a color map depending on both V_G and N_l in Figure 3a. The low-energy region of $U(N_l, V_G)$ is seen to correspond precisely to the equilibrium density defined by Equation (5) (as expected). Excursions from equilibrium, as shown by the magenta dots, thus push the system to higher energy. The energy landscape of Figure 3a is consistent with the experimentally observed tendency of the system to relax back down in energy to the equilibrium configuration.

A more dramatic example of nonequilibrium behavior is shown in **Figure 4** which exhibits the time evolution of a nonequilibrium melting process at a molecular solid–liquid interface. The STM image in Figure 4a shows the equilibrium configuration of this area at $V_G = -20$ V after sufficiently long

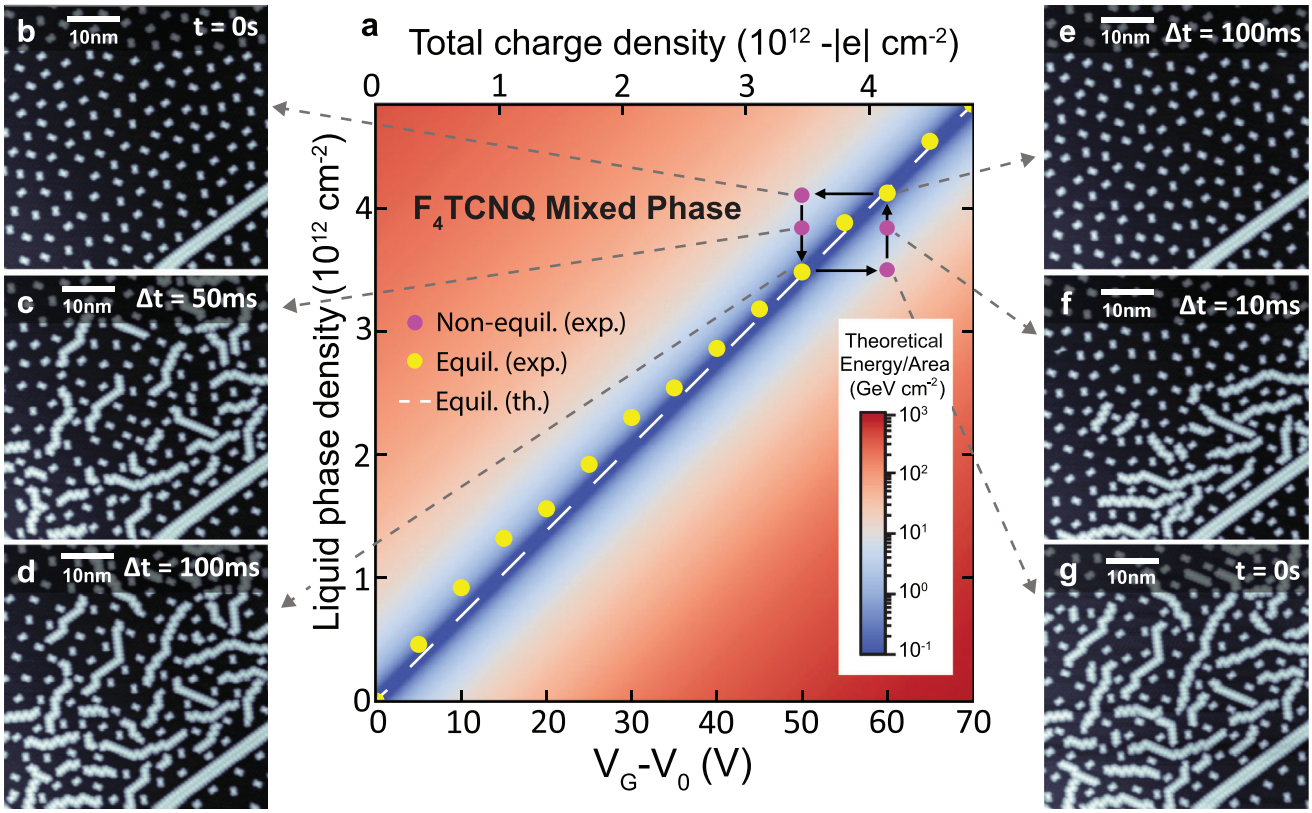

Figure 3. F_4TCNQ chain freezing and melting under nonequilibrium conditions. a) Experimental values of the equilibrium liquid phase molecule density (N_l/A) are plotted as yellow dots and nonequilibrium values as magenta dots. The theoretical total energy of the equilibrium mixed phase of F_4TCNQ/graphene is also shown (color scale) as a function of liquid phase surface density and gate voltage (V_0 is the gate voltage at which melting first begins). The minimum energy configuration corresponds to the dashed white line (obtained from Equation (5)). b) STM image of the nonequilibrium molecular state obtained by switching $V_G - V_0$ to 50 V starting from the equilibrium state at $V_G - V_0 = 60$ V and not allowing the system to evolve under diffusive conditions ($t = 0$). c) Molecular chains condense into a nonequilibrium state after allowing the system to evolve for 50 ms under diffusive conditions ($I_{SD} = 1.1$ mA, $V_G - V_0 = 50$ V). d) Molecular chain condensation advances to this equilibrium state after waiting an additional 50 ms under diffusive conditions ($I_{SD} = 1.15$ mA, $V_G - V_0 = 50$ V). e) STM image of the nonequilibrium state obtained by switching $V_G - V_0$ to 60 V and not allowing the system to evolve under diffusive conditions ($t = 0$). f) Molecular chains have partially melted in this nonequilibrium state obtained after allowing the system to evolve for 10 ms under diffusive conditions ($I_{SD} = 1.11$ mA, $V_G - V_0 = 60$ V). g) Molecular chains have melted even further in this equilibrium state obtained after waiting an additional 90 ms under diffusive conditions ($I_{SD} = 1.11$ mA, $V_G - V_0 = 60$ V), thus returning the molecular density to its initial configuration in (b). STM images were obtained at $T = 4.5$ K.

diffusive conditions. A region of high solid phase density can be seen in the upper left and zero liquid phase density throughout. The surface was then put into a nonequilibrium state by rapidly changing the gate voltage to $V_G = 60$ V (corresponding to a high liquid phase density equilibrium target). The system was then allowed to evolve under diffusive conditions for only $\Delta t = 500$ µs before being quenched and imaged as shown in Figure 4b. This nonequilibrium snapshot shows a "wave" of liquid phase molecules emanating from the molecular solid like water from a melting glacier. The width of the liquid layer extends outward from the solid by ≈80 nm and exhibits an interparticle spacing that is mostly constant. Figure 4c shows the same area after allowing it to evolve under diffusive conditions for another 700 µs. The layer of liquid now extends outward from the solid by more than 160 nm. A full video of this process can be found in Movie S3 (Supporting Information).

The theoretical framework discussed up to now is inadequate to model this type of nonequilibrium dynamics. To better understand this melting process we have generalized our overall model to account for: i) multiple chains, ii) isolated uncharged molecules, and iii) screened Coulomb interactions between charged molecules. We have numerically simulated this more complete model using the Monte Carlo method (see Section 6, Supporting Information) to explain the dynamics shown in Figure 4a–c. An initial configuration was chosen with molecules arranged into chains (Figure 4d), similar to the F_4TCNQ solids we observe experimentally. All model parameters were constrained by the experiment except for α (for which we only have an upper bound), but our results do not strongly depend on the precise value of α. A fixed number of electrons was added to the system at the start of the calculation to simulate the gating process, and the resulting liquid phase density and E_F value were subsequently determined. Overall, the simulation produced results quite similar to the experiment. For example, isolated molecules were observed to dissociate from chains after only a few Monte Carlo steps and to move toward empty graphene

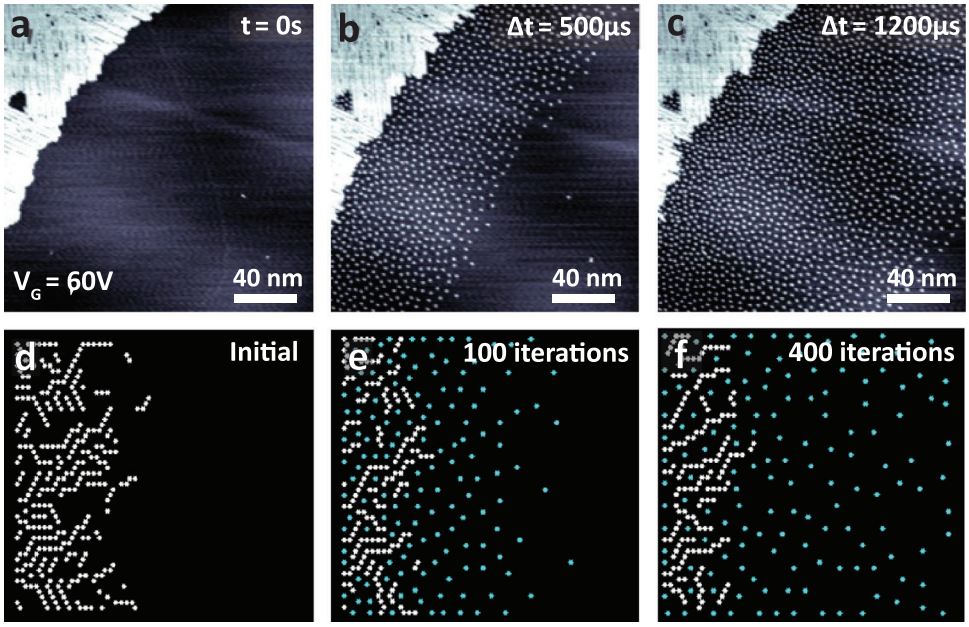

Figure 4. Nonequilibrium melting of the F_4TCNQ solid. a) STM image of an equilibrium F_4TCNQ solid formed under diffusive conditions on a graphene FET at $V_G = -20$ V. V_G was stepped up to $V_G = 60$ V before imaging, but the system was not allowed to evolve under diffusive conditions ($t = 0$). b) Same region of the surface after allowing it to evolve under diffusive conditions for $\Delta t = 500$ μs ($I_{SD} = 1.3$ mA, $V_G = 60$ V). A "wave" of charged liquid phase molecules can be seen emanating from the solid interface. c) Same region after allowing the system to evolve for an additional $\Delta t = 700$ μs under diffusive conditions ($I_{SD} = 1.3$ mA, $V_G = 60$ V). The flow of charged molecular liquid has extended even further from the condensed phase interface. d–f) Monte Carlo simulations of F_4TCNQ molecules disassociating from chains to model the behavior shown in (a–c). Molecules colored in blue are charged and can be seen flowing outward from the charge-neutral condensed phase interface. STM images were obtained at $T = 4.5$ K.

regions (Figure 4e,f), similar to the flow of molecules observed experimentally in Figure 4b,c.

3. Conclusion

We have observed a gate-tunable first-order solid–liquid phase transition for F_4TCNQ molecules adsorbed onto the surface of a graphene FET. We are able to control and image the relative abundances of liquid and solid phases for different equilibrium conditions and to directly visualize nonequilibrium processes with a single-molecule resolution for both the solid and liquid phases. We have developed an analytical model that explains the gate-dependent equilibrium properties of this system with the only unknown parameter being the energy of cohesion of the molecular solid. The techniques described here provide a new method for experimentally extracting this parameter, and our results put an experimental upper bound on it of 40 meV per molecule. Monte Carlo simulations show reasonable agreement with the highly nonequilibrium kinetics observed in our experiment. The phenomenology observed here should be generalizable to other adsorbate/surface systems that are similarly gate-tunable.

4. Experimental Section

Graphene Transistor Fabrication: Graphene/hexagonal boron nitride (hBN) FETs were fabricated on highly doped SiO_2/Si by mechanical exfoliation. Electrical source and drain contacts were fabricated by depositing 3 nm thickness of Cr and 10 nm thickness of Au through a stencil mask. The doped silicon substrate was used as the back gate. After placing in UHV, the graphene surface was cleaned by high-temperature annealing in a vacuum at 400 °C for 12 h.

Molecule Deposition: F_4TCNQ molecules were loaded into a Knudsen cell evaporator and heated to 120 °C under ultrahigh-vacuum (UHV) conditions for deposition onto a graphene FET held at room temperature. Sub-monolayer molecular coverage was achieved by keeping the deposition time under 15 s.

STM/STS Measurements: STM/STS measurements were performed under UHV conditions at $T = 4.5$ K using a commercial Omicron LT STM with Pt/Ir tips. STM topography was obtained in constant-current mode. STM tips were calibrated on an Au(111) surface by measuring the Au(111) Shockley surface state before all STS measurements. STS was performed under open feedback conditions by lock-in detection of the tunnel current driven by a wiggle voltage having a magnitude of 6–16 V rms at 401 Hz added to the tunneling bias. WSxM software was used to process all STM and AFM images.

Supporting Information

Supporting Information is available from the Wiley Online Library or from the author.

Acknowledgements

This work was supported by the U.S. Department of Energy, Office of Science, Office of Basic Energy Sciences, Materials Sciences and Engineering Division (DE-AC02-05-CH11231), within the Nanomachine program (KC1203 which provided for STM imaging, spectroscopy, and analysis). Support was also provided by the Molecular Foundary at LBNL funded by the U.S. Department of Energy, Office of Science, Office of Basic Energy

Sciences, Scientific User Facilities Division (DE-AC02-05CH11231), which provided for graphene device fabrication; by the National Science Foundation Award CHE-2204252 (molecular deposition and characterization); by the EPSRC grant EP/S025324/1 (calculation of molecular vdW bonding energy from DFT); by the Thomas Young Centre under grant number TYC-101 (Monte Carlo simulations); by the Imperial College London Research Computing Service (DOI: 10.14469/hpc/2232) (DFT calculation of molecular chain electronic structure); and by JSPS KAKENHI Grant Number 20H00354, 21H05233, and 23H02052 and World Premier International Research Center Initiative (WPI), MEXT, Japan. (growth of hBN crystals). F.L. acknowledges support from a Kavli Ensi Philomathia Graduate Student Fellowship. Z.G. was supported through a studentship in the Centre for Doctoral Training on Theory and Simulation of Materials at Imperial College London funded by the EPSRC (EP/L015579/1). We thank J.M. Kahk for useful discussions.

Note: The marking for the three corresponding authors, as Alex Zettl, Johannes Lischner, and Michael Crommie, was clarified on September 27, 2023, after initial publication online, following a misunderstanding and a technical issue in the proofing process.

Conflict of Interest

The authors declare no conflict of interest.

Author Contributions

F.L. and H.-Z.T. contributed equally to this work. Conceptualization was done by F.L., H.-Z.T., A.A., and M.C.; Methodology was done by F.L., H.-Z.T., A.A., Z.G., and J.L.; Investigation was done by F.L., H.-Z.T., A.A., E.H., M.H., K.W., T.T., and M.C.; Visualization was done by F.L., H.-Z.T., A.A., and Y.Y.; Funding acquisition was done by J.L. and M.C.; Project administration was done by J.L. and M.C.; Supervision was done by J.L. and M.C.; Writing was done by F.L., H.-Z.T., Z.G., J.L., and M.C.; Review and editing were written by F.L., H.-Z.T., Z.G., J.L., and M.C.

Data Availability Statement

The data that support the findings of this study are available from the corresponding author upon reasonable request.

Keywords

field-driven phase transitions, graphene field-effect transistor, molecular solids, nonequilibrium dynamics, solid–liquid phase coexistence

Received: January 17, 2023
Revised: June 6, 2023
Published online: July 13, 2023

[1] H. Guo, K. Chen, Y. Oh, K. Wang, C. Dejoie, S. A. Syed Asif, O. L. Warren, Z. W. Shan, J. Wu, A. M. Minor, *Nano Lett.* **2011**, *11*, 3207.
[2] K.-A. N. Duerloo, Y. Li, E. J. Reed, *Nat. Commun.* **2014**, *5*, 4214.
[3] S. Song, D. H. Keum, S. Cho, D. Perello, Y. Kim, Y. H. Lee, *Nano Lett.* **2016**, *16*, 188.
[4] W. Li, L. Kong, B. Feng, H. Fu, H. Li, X. C. Zeng, K. Wu, L. Chen, *Nat. Commun.* **2018**, *9*, 198.
[5] C. Liu, S. Yamazaki, R. Hobara, I. Matsuda, S. Hasegawa, *Phys. Rev. B* **2005**, *71*, 041310.
[6] K. F. Mak, J. Shan, D. C. Ralph, *Nat. Rev. Phys.* **2019**, *1*, 646.
[7] H. Kuwahara, Y. Tomioka, A. Asamitsu, Y. Moritomo, Y. Tokura, *Science* **1995**, *270*, 961.
[8] F. Zhang, H. Zhang, S. Krylyuk, C. A. Milligan, Y. Zhu, D. Y. Zemlyanov, L. A. Bendersky, B. P. Burton, A. V. Davydov, J. Appenzeller, *Nat. Mater.* **2019**, *18*, 55.
[9] B. Wortmann, D. V Vörden, P. Graf, R. Robles, P. Abufager, N. Lorente, C. A. Bobisch, R. Möller, *Nano Lett.* **2016**, *16*, 528.
[10] J. Crossno, J. K. Shi, Ke Wang, X. Liu, A. Harzheim, A. Lucas, S. Sachdev, P. Kim, T. Taniguchi, K. Watanabe, T. A. Ohki, K. C. Fong, *Science* **2016**, *351*, 1058.
[11] M. Kühne, F. Börrnert, S. Fecher, M. Ghorbani-Asl, J. Biskupek, D. Samuelis, A. V. Krasheninnikov, U. Kaiser, J. H. Smet, *Nature* **2018**, *564*, 234.
[12] T. Nakamuro, M. Sakakibara, H. Nada, K. Harano, E. Nakamura, *J. Am. Chem. Soc.* **2021**, *143*, 1763.
[13] A. Alessandrini, P. Facci, *Soft Matter* **2014**, *10*, 7145.
[14] F. Liou, H.-Z. Tsai, A. S. Aikawa, K. C. Natividad, E. Tang, E. Ha, A. Riss, K. Watanabe, T. Taniguchi, J. Lischner, A. Zettl, M. F. Crommie, *Nano Lett.* **2021**, *21*, 8770.
[15] J.-P. Hansen, I. R. McDonald, in *Theory of Simple Liquids*, 3rd ed., Academic Press, Amsterdam, The Netherlands **2006**, pp. 46–77.
[16] Y. Zhang, V. W. Brar, F. Wang, C. Girit, Y. Yayon, M. Panlasigui, A. Zettl, M. F. Crommie, *Nat. Phys.* **2008**, *4*, 627.
[17] S. Wickenburg, J. Lu, J. Lischner, H.-Z. Tsai, A. A. Omrani, A. Riss, C. Karrasch, A. Bradley, H. S. Jung, R. Khajeh, D. Wong, K. Watanabe, T. Taniguchi, A. Zettl, A. H. C Neto, S. G. Louie, M. F. Crommie, *Nat. Commun.* **2016**, *7*, 13553.
[18] R. Decker, Y. Wang, V. W. Brar, W. Regan, H.-Z. Tsai, Q. Wu, W. Gannett, A. Zettl, M. F. Crommie, *Nano Lett.* **2011**, *11*, 2291.
[19] D. A. Rehn, Y. Li, E. Pop, E. J. Reed, *npj Comput. Mater.* **2018**, *4*, 2.
[20] A. H. Castro Neto, F. Guinea, N. M. R. Peres, K. S. Novoselov, A. K. Geim, *Rev. Mod. Phys.* **2009**, *81*, 109.
[21] M. Kim, J. R. Chelikowsky, *Appl. Phys. Lett.* **2015**, *107*, 163109